ACSNANO

www.acsnano.org

ARTICLE

Flash Graphene Morphologies

Michael G. Stanford, Ksenia V. Bets, Duy X. Luong, Paul A. Advincula, Weiyin Chen, John Tianci Li, Zhe Wang, Emily A. McHugh, Wala A. Algozeeb, Boris I. Yakobson,* and James M. Tour*

Cite This: *ACS Nano* 2020, 14, 13691−13699

Read Online

ACCESS | Metrics & More | Article Recommendations | Supporting Information

ABSTRACT: **Flash Joule heating (FJH) can convert almost any carbon-based precursor into bulk quantities of graphene. This work explores the morphologies and properties of flash graphene (FG) generated from carbon black. It is shown that FG is partially comprised of sheets of turbostratic FG (tFG) that have a rotational mismatch between neighboring layers. The remainder of the FG is wrinkled graphene sheets that resemble nongraphitizing carbon. To generate high quality tFG sheets, a FJH duration of 30−100 ms is employed. Beyond 100 ms, the turbostratic sheets have time to AB-stack and form bulk graphite. Atomistic simulations reveal that generic thermal annealing yields predominantly wrinkled graphene which displays minimal to no alignment of graphitic planes, as opposed to the high-quality tFG that might be formed under the direct influence of current conducted through the material. The tFG was easily exfoliated via shear, hence the FJH process has the potential for bulk production of tFG without the need for pre-exfoliation using chemicals or high energy mechanical shear.**

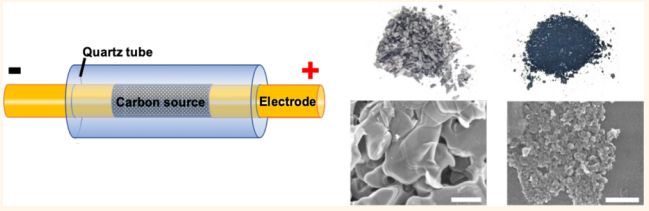

KEYWORDS: *flash Joule heating, graphene, turbostratic graphene, graphene morphology, FJH*

Graphene is a 2-dimensional sheet of sp^2-hybridized carbon.[1,2] Because of the stable carbon−carbon covalent bonding and sp^2-hybridization, graphene exhibits high carrier mobility,[3] thermal conductivity,[4] and mechanical strength, among other favorable properties.[5] Graphene is typically synthesized by chemically or mechanically intensive top-down methods[6] or slow bottom-up methods.[2,7] Top-down approaches often start with bulk graphite that is subsequently exfoliated into sheets by mechanical, electrochemical, or chemical processes, such as via the production of graphene oxide with subsequent reduction. Bottom-up graphene growth is usually carried out by chemical vapor deposition (CVD), which is suitable for the growth of single to few-layer graphene films. However, CVD growth typically results in small quantities of graphene and is not a suitable method for bulk graphene production, where a large mass of graphene is desired.

Arc discharge[8] and pulsed wire discharge[9] have been demonstrated as electrical methods to generate graphene or AB-stacked graphene nanoplatelets. However, these methods generate graphene from exfoliation of bulk graphite, and not by a bottom up synthesis. Recently, bulk quantities of flash graphene (FG) have been generated in a process by which virtually any carbon source is converted to graphene using flash Joule heating (FJH).[10] The FG is largely turbostratic, which facilitates ease in exfoliation and dispersibility. The turbostratic FG (tFG) is significantly mechanically, electronically, and optically decoupled from neighboring sheets, resulting in spectroscopic signatures similar to high-quality monolayer graphene. The high-power FJH rapidly heats the carbon precursor and causes outgassing of noncarbon elements. Rapid cooling prevents rotational registration of graphene sheets and promotes the formation of tFG sheets. In this work, the production and morphology of FG are studied. The mechanism is explored by which turbostratic sheets are assembled.

RESULTS/DISCUSSION

To synthesize FG, carbon black (CB) was enclosed within a quartz tube and pressed between two copper electrodes with copper wool physically touching the CB, as shown in Figure 1a. The electrodes were connected to a capacitor bank with a total capacitance of 60 mF and charged to a voltage of 120 V. A schematic of the flash Joule heating system can be found in Figure S1. Controlled discharge of the capacitor banks through the CB results in FJH that rapidly heats the CB to ∼3000 K within tens of ms and then it cools to room temperature within seconds.[10] During the discharge time period, the CB is rapidly heated and graphitized to form FG, as illustrated in Figure 1b. Figure 1c reports the current and voltage across the CB for a

Received: July 15, 2020
Accepted: September 10, 2020
Published: September 10, 2020

https://dx.doi.org/10.1021/acsnano.0c05900
ACS Nano 2020, 14, 13691−13699

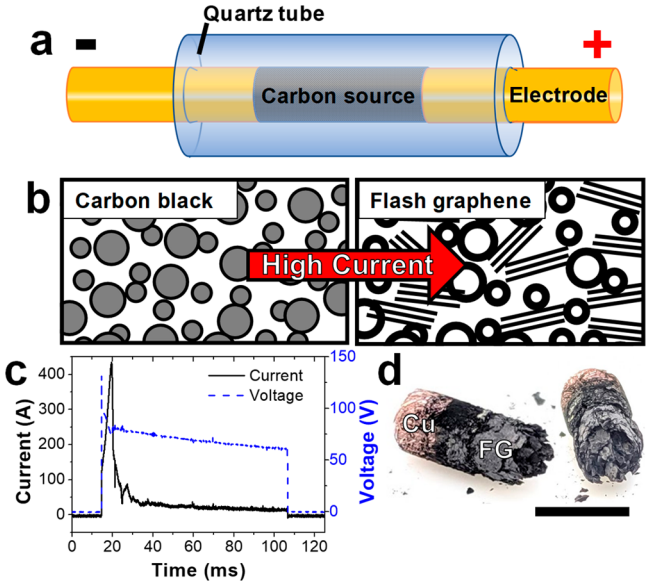

Figure 1. General FJH characteristics. (a) Schematic setup for FJH of a carbon source to form FG. (b) Schematic representing the graphitization of the carbon source after FJH. In the product (right), the circles represent graphitized carbon. The lines represent FG sheets. (c) Current through and voltage across the carbon source during FJH is complete in the millisecond time scale. (d) Photograph of FG after FJH as it was pushed from the quartz tube and broken in two. Copper wool was used as an electrode, but this is easily substituted with a refractory conductor such as graphite rods. Scale bar is 5 mm.

FJH duration of 100 ms. Notably, a peak current of >400 A passes through the CB that results in a rapid power dissipation of ~30 kW. This high-power dissipation is responsible for the rapid FJH. During FJH, the CB forms planar crystals of tFG that are aligned in the direction of current and resemble a charred log (Figure 1d). The CB starting material is predominantly comprised of small particles that are largely amorphous carbon with small graphitic domains. After 100 ms of FJH, sheets of tFG are dispersed throughout the sample along with small graphitized carbon particles, thus resulting in the bulk bottom-up synthesis of graphene.

High-resolution transmission electron microscopy (HR-TEM) was conducted to observe the atomic structure of FG, and Figure 2a shows tFG sheets. A slight rotational mismatch between sheets (denoted by the nonparallel inset white dotted lines), results in a moiré pattern that manifests itself as striations in the image only where the mismatched sheets overlap. The rotational mismatch between these sheets is ~5.4°. The moiré pattern induced by the rotational mismatch is more clearly shown in Figure 2b. Figure 2c shows similar striations in the image due to a rotational mismatch between neighboring sheets of graphene. The rotational mismatch is further analyzed in an image in Figure S2. As depicted in Figure 1b, a FG sample is composed of sheets of tFG as well as smaller particles of graphitic carbon. The HR-TEM images of the smaller particles are shown in Figure 2d and e. This material is graphitic with many bends and typically has a thickness of 3−8 layers.[10] It resembles nongraphitizing carbon[11,12] and will be referred to as wrinkled graphene in this work. TEM images of both forms of graphene reveal an interatomic spacing of ~0.34 nm, which corresponds with turbostratic material and lack of AB-stacking (Figure S3).

Upon synthesizing FG, the sample is comprised of gray crystals and a fine black powder, as shown in Figure 3a, and the combined yield is ~85% by weight. The two components can easily be separated by screen-sieving since the gray crystals coalesce into larger particles. Additionally, separation techniques such as centrifugation may be applied to purify the products. SEM imaging reveals that the gray crystals (Figure 3b) are extended networks of tFG sheets that readily exfoliate and delaminate, whereas the fine black powder is the wrinkled graphene. Representative Raman spectra of the tFG sheets and wrinkled graphene are shown in Figure 3d. The wrinkled graphene is further characterized by a 2D/G ratio of ~1.1 and

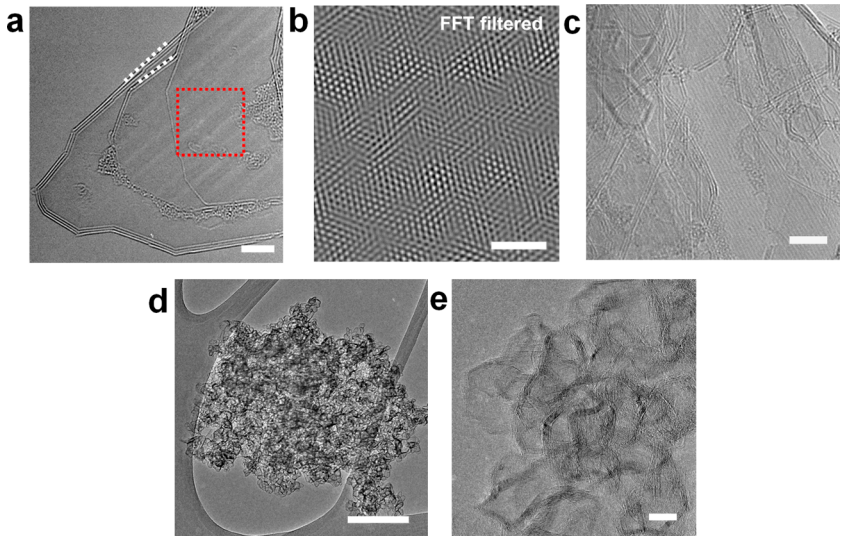

Figure 2. Microscopic analysis of the FJH products. (a) TEM image of tFG sheets with striations in the image denoting rotational mismatch. A portion of the red boxed region is further studied in panel b. Scale bar is 5 nm. (b) FFT filtered image of the inset region in a revealing a moiré pattern. Scale bar is 2 nm. (c) TEM image of tFG showing more striations indicating a rotational mismatch. Scale bar is 5 nm. (d) TEM image of wrinkled graphene produced from the FJH procedure. Scale bar is 200 nm. (e) HR-TEM image of the wrinkled graphene. Scale bar is 10 nm.

https://dx.doi.org/10.1021/acsnano.0c05900
ACS Nano 2020, 14, 13691−13699

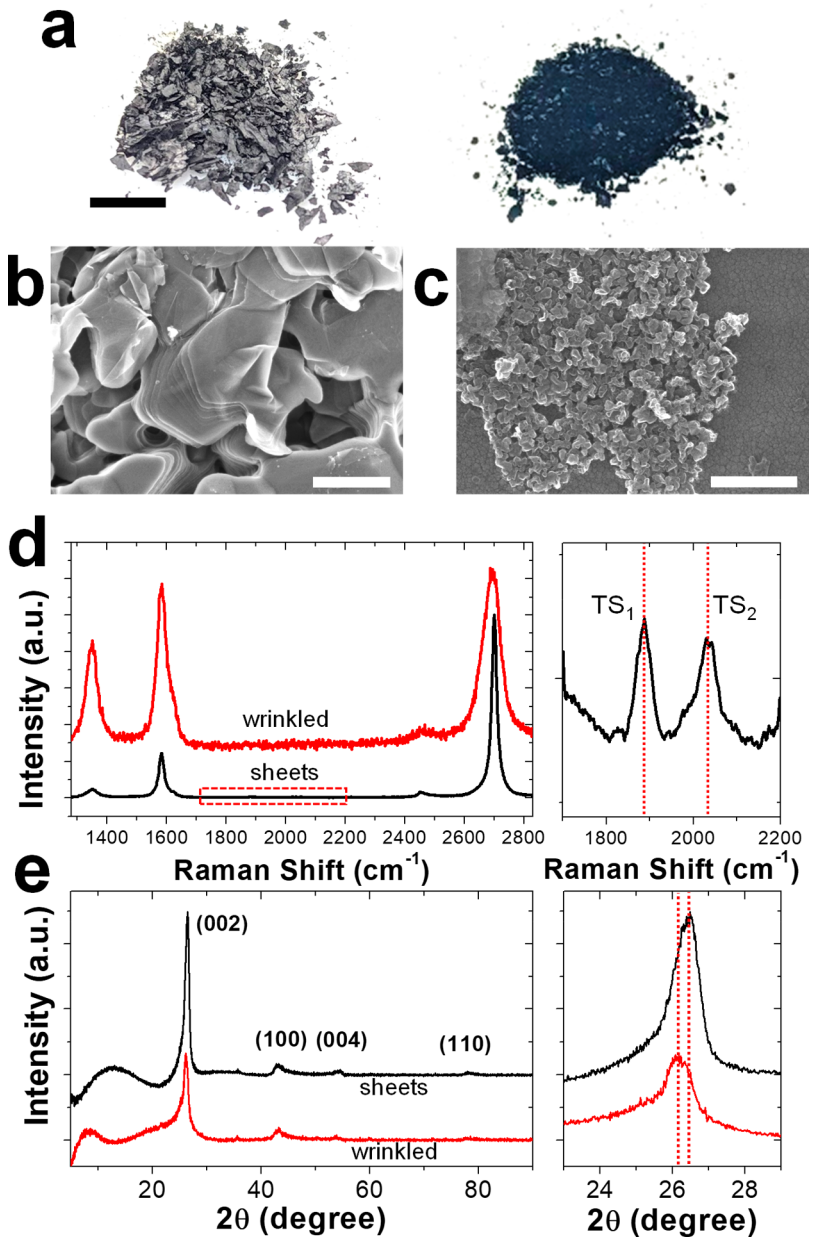

Figure 3. FJH product morphologies and spectral characteristics. (a) Photographs of FG that was passed through a 250 μm sieve. Gray crystals are separated from a fine black powder. The scale bar is 3 mm. (b) SEM image of the gray crystals showing delaminating sheets. Scale bar is 500 nm. (c) SEM image of the black powder that is comprised of nanoparticles. Scale bar is 300 nm. (d) Representative Raman spectra for sheets and wrinkled structures. Expansion of the red boxed region from the sheets (right) exhibit TS_1 and TS_2 peaks that are characteristic of turbostratic layers and show a missing M band. (e) X-ray diffraction of sheets and wrinkled structures. A shift in the peak position of (002) peak is exhibited for the wrinkled structures.

a large D peak, presumably due to extensive curvature of the wrinkled graphene.[13] The tFG sheets exhibit a much larger 2D/G ratio with a minimal D peak. The tFG sheets also have distinct TS_1 and TS_2 peaks confirming that the FG is indeed turbostratic. These peaks only arise due to rotational mismatch between neighboring layers of graphene.[10,14] A more thorough analysis of the Raman spectra with peak fitting is provided in the Figures S4 and S5. X-ray diffraction for each morphology is shown in Figure 3e. An asymmetric (002) peak is exhibited along with a weak (100) peak. These characteristics are typically exhibited in turbostratic graphene.[15,16] The (002) peak for tFG sheets is more pronounced than in the wrinkled graphene, which suggests a larger crystallite size in the *c*-axis. This is evident by observing the SEM image in Figure 3b that reveals the crystals of tFG sheets may be many layers thick and on the order of microns. Figure S6 shows cross-sectional SEM images of the tFG crystals.

The drastic difference in morphology of tFG and wrinkled graphene suggest nonuniform formation conditions. Using molecular dynamics simulation with AIREBO potential (see SI for details), we analyzed the process and results of the fast high-temperature annealing of CB material as shown in Figure 4. The initial structure was designed to contain ~66% of centroid particles characteristic for CB and ~34% of loose amorphous carbon and surrounded by graphitic walls to emulate the presence of quartz walls during the FJH process

https://dx.doi.org/10.1021/acsnano.0c05900
ACS Nano 2020, 14, 13691−13699

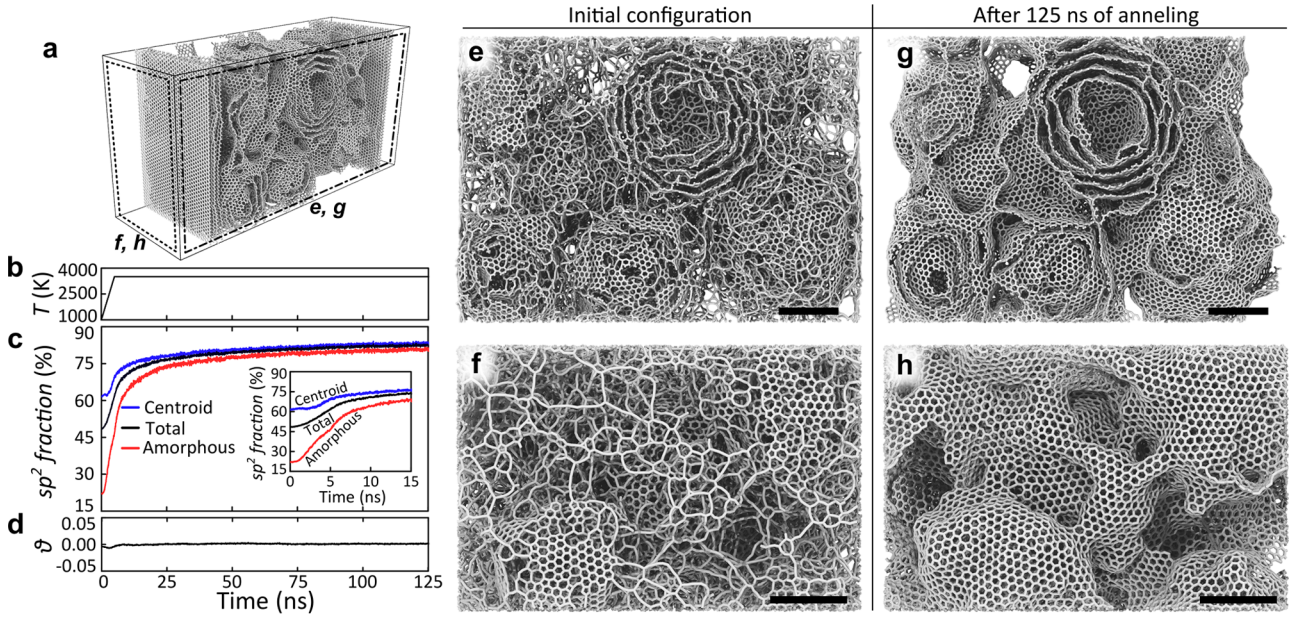

Figure 4. Modeling of flash graphene formation. (a) Structure of the amorphous carbon used for a molecular dynamics simulation of high-temperature annealing; vertical graphitic walls can be seen toward the front and back of the frame. (b) The temperature profile, (c) graphitization level, and (d) Herman's orientation function during the annealing. Visual comparison of (e, f) the initial configuration at two different locations and (g, h) final configurations at the same two different locations, showing a significant level of graphitization after annealing. Direction of view is through the large front face in panel a, graphitic walls are omitted. Interestingly, the fraction of the sp^2-hybridized carbon within the centroid particles changes significantly less compared to amorphous material (c), indicating an increased annealing barrier for atoms within the preexisting graphene-like structure. At the same time, the orientation function (d) shows no significant reorientation or alignment of graphitic structures despite the presence of walls. Scale bars are 2 nm.

(Figure 4a). After initial pretreatment at 1000 K for 5 ns, the material was exposed to heating and consequent annealing at a constant temperature of 3500 K (Figure 4b), while graphitization (Figure 4c) and Herman's orientation function (Figure 4d) of the material was monitored. As expected, the graphitization level, specifically the fraction of carbon atoms in the sp^2-configuration, significantly increases from ∼60% to ∼85% during the annealing process, with the most significant change occurring during the initial heating period (Figure 4c inset). Interestingly, the material within centroid particles appears to be significantly less mobile compared to the loose amorphous carbon resulting in smaller graphitization increase due to slow annealing of defects trapped in graphene-like centroid shells. At the same time, surrounding amorphous carbon does not have a rigid pre-existing structure and undergoes rapid graphitization resulting in the formation of graphene-like coating covering centroid particles (Figure 4e–h). Taking experimental observations as a guide, we analyzed the alignment of graphitic domains within the structure during annealing using Herman's orientation function θ, commonly used in polymer science. Computed as $\theta = (3\langle\cos^2\alpha\rangle - 1)/2$, where α is an angle between the normal to the local direction of the graphitic plane and the characteristic direction chosen to be horizontal (see SI for details and Figure S7), the orientation function is expected to be equal to 1, −0.5, and 0 for domains aligned with graphitic walls, perpendicular to the walls and randomly oriented, respectively. No significant change of alignment is observed during the annealing process (Figure 4d), mainly preserving the value dictated by the initial configuration. Even prolonged thermal annealing at high temperatures (125 ns, 3500 K) does not show a structural change characteristic for the formation of tFG by FJH; only wrinkled graphene is observed (Figures 3c and 4h). From these observations, we can conclude that wrinkled graphene forms at the areas of material undergoing simple thermal annealing. At the same time, the current and its directionality might guide formation of tFG.

On the basis of the thermal simulations and experimental observations, we are able to speculate on the formation of the two distinct FG morphologies. The difference arises from the preexisting morphology of CB containing characteristic centroid particles (composed of concentric graphitic shells) and surrounding amorphous carbon that does not display any overarching morphology (Figure 4e, f). At the voltage application, the current would be conducted following the path of lowest resistance, thereby supplying the largest amount of heat to the conducting areas. The material on and surrounding the conduction path would experience significant annealing and graphitization, progressively increasing the conductance. Nearby localized defects and less conductive domains would continue being heated and thereby annealed out due to increased scattering leading to the elimination of defects. The material as a whole would undergo transformation leading to the formation of more conductive channels of tFG sheets. This formation is likely facilitated through highly mobile amorphous carbon. Conversely, centroid particles cannot facilitate current conductance. As a result, material composing the centroid particles would undergo only slow thermal defect annealing. This distinction is akin to the morphology-based nongraphitizing nature of the glassy carbons proposed in the literature.[17,18] Being enclosed in a continuous sp^2-carbon network within each centroid shell, atoms remain in a locally favorable configuration and show very low mobility. A global structural transformation associated with a significant energy barrier is necessary to convert such a network into a sheet form. Additionally, the amorphous carbon

https://dx.doi.org/10.1021/acsnano.0c05900
ACS Nano 2020, 14, 13691−13699

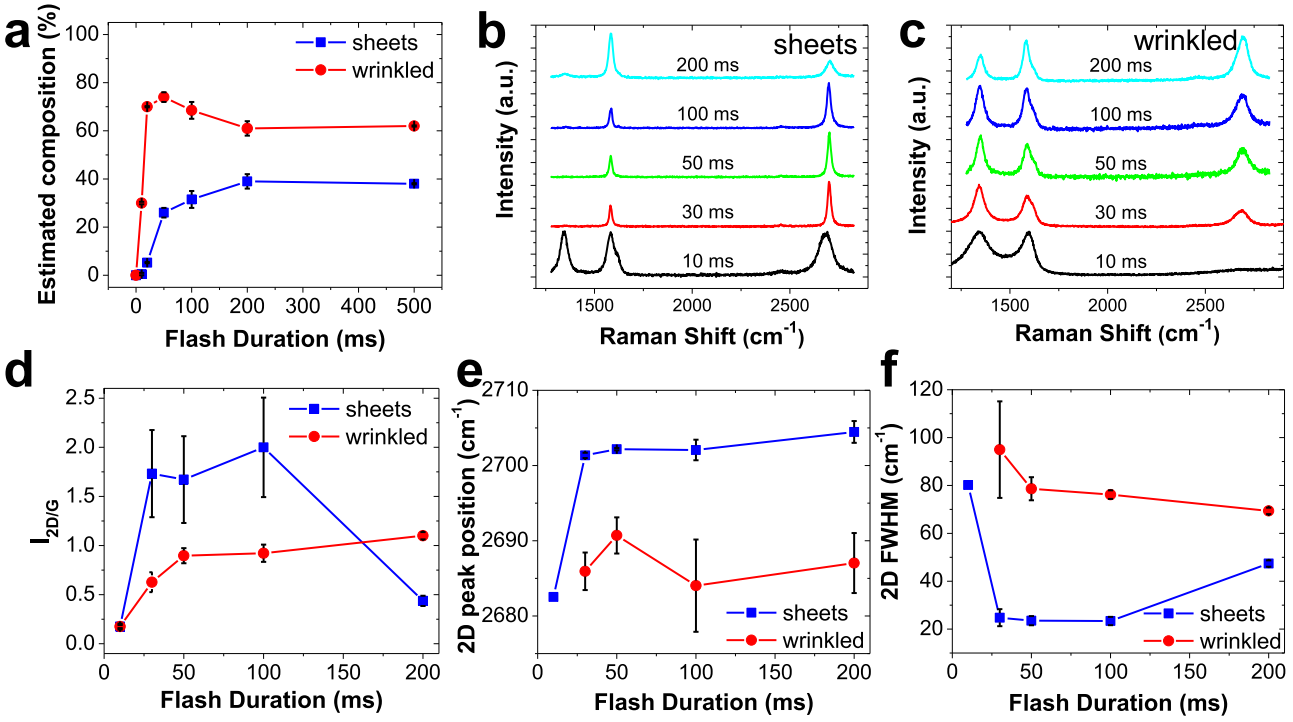

Figure 5. Effect of flash time duration on graphene morphology. (a) Estimated composition of a batch of FG as a function of FJH flash duration. (b) Representative Raman spectra at various flash durations for (b) tFG sheets and (c) wrinkled graphene. Analysis of Raman spectra reporting the (d) 2D/G intensity ratio, (e) 2D peak position, and (f) 2D fwhm. The error bars represents the standard deviation where $N = 10$.

outside of the conductance path is likely to adhere to the centroid particles and go through a limited graphitization, similar to that observed in thermal simulations (Figure 4). As a result, material outside of the conductance path, including both centroid particles and amorphous carbon, forms wrinkled graphene.

These conjectures are consistent with experimental observations of the high percentage of tGH sheets resulting from flashing carbon sources containing a large amount of amorphous carbon (i.e., coffee grounds).[10] At the same time previously processed and filtered wrinkled graphene shows minimal conversion to tFG sheets during repeated subjection to FJH (Figure S8) suggesting strong correlation between the amount of the amorphous carbon in the initial material and the fraction of carbon source converted to tFG sheets.

By controlling the flash duration through electrical pulse cessation during which FG is generated, the composition and morphology of FG can be tuned. Using an image analysis technique and Raman spectra (Figure S9), the amount of tFG sheets and wrinkled graphene is estimated as a function of the flash duration in Figure 5a. At $t = 0$ ms, the entire batch of material is amorphous carbon. Upon FJH, tFG sheets and wrinkled graphene are produced. The amount of tFG sheets increases relative to wrinkled graphene until ~200 ms of pulse is applied. Beyond 200 ms, the composition of tFG sheets remains unchanged. Figure 5b and c shows representative Raman spectra for the tFG sheets and wrinkled graphene. Complementary SEM images of the material are reported in Figures S10 and S11. Notably, tFG sheets exhibit much narrower peak full-width at half-maximum (fwhm) and more pronounced 2D peaks. Analysis of the Raman spectra for FG morphologies is reported in Figure 5d and f. The 2D/G ratio gives a reflection of graphene quality, and generally higher 2D/G ratio is exhibited by high quality graphene with low defect concentration. For the wrinkled graphene, the 2D/G ratio increases with flash duration and largely saturates beyond 100 ms once full graphitization has occurred. For the tFG sheets, the average 2D/G ratio is ~1.8 to 2.0 up to 100 ms; however, the 2D/G ratio decreases to ~0.4 with a flash duration of 200 ms and beyond. These results indicate that rotationally decoupled tFG is formed during short flash durations (30–100 ms). When prolonged FJH is supplied (200 ms), the tFG sheets begin to AB-stack toward a graphite morphology, as confirmed by the reduction in 2D/G ratio and the increase in 2D fwhm. Figure 5e shows the position of the 2D peak. Once the tFG sheets begin to form and planarize, the 2D peak shifts from ~2683 cm^{-1} to 2701 cm^{-1}. Figure 5f reports the fwhm of the 2D peak for the tFG sheets and wrinkled graphene. Between 30 to 100 ms pulse duration, the tFG sheets exhibit a narrow fwhm averaged ~23 cm^{-1} that can be fitted with a single Lorentzian. This optically decoupled behavior is similar to the fwhm of a single layer of graphene. Therefore, modulation of the FJH conditions yield differing compositions according to the desired product. Additional images and Raman spectra of tFG sheets, wrinkled graphene, and other morphologies formed can be found in Figures S12–S18. Some regions from a batch of FG formed densely packed graphite polyhedral crystals (GPCs). Figure S15 shows that the GPCs form faceted rods. The Raman spectra typically displayed a 2D/G ratio of ~1.0. Figure S16 shows more images of various GPC morphologies ranging from cones to high aspect-ratio rods.

Figure 6 shows SEM images taken from various regions of tFG that show the progression of tFG formation. These images were collected along the surface of a single crystal of tFG, which was presumably exposed to a temperature gradient. In

https://dx.doi.org/10.1021/acsnano.0c05900
ACS Nano 2020, 14, 13691–13699

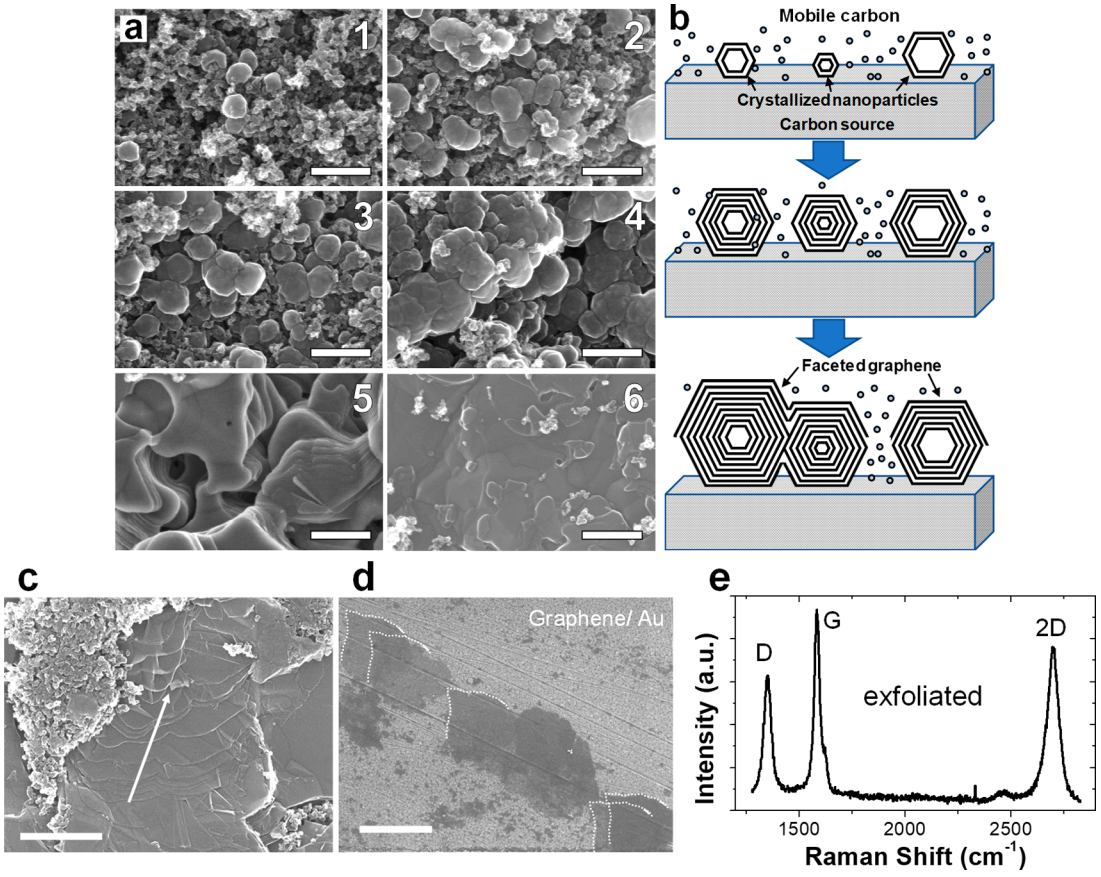

Figure 6. Morphology growth patterns. (a) SEM images (1−6) showing nucleation and growth of graphitic crystals across the surface of a bed of graphitic nanoparticles. Crystals merge and eventually form a continuous graphitic shell. All scale bars are 300 nm. (b) Schematic proposed mechanism for the formation of FG on the surface of graphitic crystals. Mobile carbon is shown as small circles. (c) SEM image of gray tFG crystal that was mechanically sheared, showing facile delamination of the bulk material. Scale bar is 500 nm. (d) Large area exfoliation of tFG upon transfer to an Au substrate (sheet edges were outlined for SEM image contrast). Scale bars is 1 μm. (e) Representative Raman of exfoliated FG.

image 1, seeds of faceted spherical particles can be seen nucleating in a bed of carbon. These seeds grow and merge in images 2−4. Eventually, layers of faceted tFG sheets form on the top of merged seeds (image 5). These regions generally exhibit the spectroscopic signatures of turbostratic graphene with Raman 2D/G ratios reaching >15 (Figure S13). With sufficient heating time, the FG sheets merge and begin to AB stack and form more continuous graphite (image 6). Figure S19 shows the effect of power dissipation during flashing on the nucleation and growth of tFG. A sharp increase in the resistance of the carbon source after ∼15 ms of flash duration suggests that the material becomes discontinuous potentially due to mobile carbon generation or gas evolution. The mobile carbon may originate from high resistance junctions between neighboring carbon particles parallel to the path of current. Previous work has shown that sublimed carbon will form turbostratic particles similar to those seen in Figure 6a.[19] Figure 6b shows a proposed mechanism for tFG formation. The carbon source for the formation of tFG is likely mobile carbon from a bed of CB. As mobile carbon is generated, faceted nanoparticles begin to nucleate. These nanoparticles will merge and eventually faceted sheets of tFG form along the top of the nucleated particles, as shown in Figure 6a(5).

Because of the increased interplanar spacing of tFG sheets, there are weaker van der Waals interactions between neighboring layers leading to more facile exfoliation. Figure 6c shows bulk crystals of tFG that were subject to shear. The crystals of tFG sheets readily delaminate due to the weak interlayer interactions. This material was exfoliated by mechanical shear between a Si wafer and Au substrate for SEM imaging clarity. Figure 6d shows that the tFG sheets are easily transferred to the Au substrate. The dotted lines in Figure 6d indicate a common edge on the graphene sheets that show these sheets were all exfoliated from the same crystal of tFG. A Raman spectrum of the exfoliated graphene is reported in Figure 6e and reveals the presence of high-quality graphene. The high D-peak is likely induced from damage to the sheet from the exfoliation process and the nonflat Au surface. The tFG can be easily exfoliated by mechanical shear (Figures S20−S24), as well as by dispersion in solutions (Figure S25).

Several other works have subjected carbon sources to Joule heating, arc discharge, or thermal shock.[20−23] However, their studies report a different morphology of the resultant material. The tFG morphology exhibited in this work may arise due to the following mechanisms: (1) flashing carbon sources with a high degree of amorphous carbon, such as CB, provides mobile carbon atoms that reform into tFG when subjected to rapid heating and cooling. This is in stark contrast to works with fully graphitized starting materials.[21,23] (2) We are achieving very high temperatures (∼3000 K) that facilitate graphitization over the span of milliseconds. This rapid heating and cooling can prevent AB-stacking and graphite formation.

https://dx.doi.org/10.1021/acsnano.0c05900
ACS Nano 2020, 14, 13691−13699

CONCLUSION

This work shows that FG is composed of turbostratic sheets of graphene (tFG) as well as wrinkled graphene as confirmed by high resolution TEM. Spectroscopically, the turbostratic sheets behave optically as monolayer graphene with high 2D/G peak ratios and narrow fwhm. The duration of FJH influences the composition of the FG and controls the ratio of tFG sheets to wrinkled graphene. Atomistic simulations reveal that thermal annealing alone would produce predominantly wrinkled graphene, with minimal alignment of graphitic planes, while high-quality tFG formation might be attributed to the direct influence of current conducted through the material. Extended FJH (>200 ms) causes the material to AB-stack moving toward a graphite morphology. Therefore, in order to generate high quality tFG, the flash duration should be maintained at ∼30−100 ms. The tFG can easily be exfoliated under shear, thus providing a method to generate bulk quantities of graphene.

METHODS

The FJH system connects a capacitor bank across a sample to rapidly discharge electrical energy into the sample. A schematic of the system is shown in Figure S1. The capacitor bank has a total capacitance of 60 mF. Discharging the capacitor banks through the carbon-rich samples results in resistive heating and rapidly increases the temperature of the sample. An IGBT was used to control the time duration of discharge (flash duration) through the sample. This enabled control of flash duration on the millisecond time scale. *Additional details and safety information on the FJH system can be found in a prior publication, and it is imperative that these safety recommendations be followed to mitigate accidental electrocution.*[10]

Evidence of Turbostratic Structure. Fast Fourier transform (FFT) of HR-TEM images reveals Bragg spots with rotational mismatch in Figure S2. Each set of 6 Bragg spots represents a single layer of FG and is indicated by the inset yellow hexagons. This region was composed of 5 sets of turbostratic FG (tFG) with rotational mismatch. Figure S3 shows HR-TEM images of tFG particles. These particles are faceted hexagonal crystals that are composed of concentric layers of graphitic carbon. The interlayer spacing was 3.4 Å, which corresponds with turbostratic graphene.

Fitted Raman Spectra. Figure S4 reports analyzed Raman spectra for tFG sheets. The TS1 and TS2 peaks confirm that the material is turbostratic. The fwhm and peak positions are inset in the image. Importantly, the G/TS ratio is only ∼55, indicating the TS1 and TS2 peaks are very pronounced. The 2D peak is centered at 2700 cm^{-1} and can be fit with a single Lorentzian peak. The fwhm is 16.4 cm^{-1}. Figure S5 reports the analyzed Raman spectra for the wrinkled graphene morphology. The TS1 and TS2 peaks are absent. The high curvature of this material may quench this peak since XRD suggests that the material is indeed turbostratic as well. The 2D peak is centered at 2695 cm^{-1} and is composed of multiple Lorentzian peaks and the fwhm is ∼60 cm^{-1}.

tFG Crystals. When forming tFG, gray tFG crystals typically form across a bed of carbon. These crystals contain many layers of tFG that are not yet exfoliated. Figure S6 shows SEM images of a crystal that was cross-sectioned with a Ga^+ beam. The tFG layers extend for tens of microns. Beneath these layers exist more tFG sheets (Figure S6d), which suggests large quantities of the material is converted to tFG sheets.

Atomistic Simulations. *Initial Structure Preparation.* Each of the characteristic CB centroid particles was constructed from individual graphitic flakes of arbitrary shape approximately 8−12 Å in diameter (Figure S7a) that are randomly positioned on concentric spherical surfaces following by random rotation and tilt (Figure S7b). Those spherical shells are combined into a centroid particle (Figure S7c), and additional individual carbon atoms are randomly positioned within the interaction range (Figure S7d). We combined eight centroid particles of various sizes (a slight deformation applied to some particles) into a large configuration adding graphitic walls and individual randomly positioned carbon atoms constituting approximately 30% of the whole structure (Figure S7e). The final configuration contained 85000 atoms. The size of the periodic cell was chosen to provide at least 15 Å of vacuum between graphitic walls.

Atomistic simulations were performed using AIREBO potential for a balance between computational cost and accuracy. Initial structure first underwent geometric optimization (some shrinkage in horizontal direction allowed for necessary change in atomic configuration) and then was subjected to preliminary annealing at 1000 K for 5×10^{-9} s to eliminate irregularities caused by the structure creation protocol.

Finally, the system was heated to the target annealing temperature with a heating speed of 0.5×10^{-12} K s^{-1} using a Nose−Hoover thermostat (canonical NVT ensemble) with a temperature damping parameter of 0.025×10^{-12} s. The structures were held at the target annealing temperatures for $\sim 125 \times 10^{-9}$ s (see temperature profile shown in Figure 4b).

Structural characteristics were collected every 10 steps of the molecular dynamics simulation. Graphitization fraction was calculated as a ratio between carbon atoms in sp^2 configuration over the total number of atoms (graphitic walls were excluded from the characterization)—Figure 4c. Additionally, graphitization fraction was calculated separately for atoms within centroid particles (Figure S7d), and the individual atoms randomly positioned around centroids (can be seen in Figure S7e). Herman's orientation function θ was employed to quantify alignment within the structure. Computed as $\theta = (3\langle\cos^2\alpha\rangle - 1)/2$, where α is an angle between the local direction of the graphitic plane and the characteristic direction. The local direction was calculated for plane formed by each sp^2 carbon atom and each combination of two of its neighbors and averaged. Generally, complete alignment with the characteristic direction would result in $\langle\theta\rangle = 1$, while alignment with the direction perpendicular to the characteristic direction should have $\langle\theta\rangle = -0.5$. To account for alignment to the plane of the graphitic walls, we chose a characteristic direction to be perpendicular to it (horizontal). Interestingly we did not observe a significant change in the alignment of the local graphitic directions nor did they become parallel to the graphitic walls nor otherwise, indicating that thermal annealing alone can not be a cause of the structural directionality observed in the experiments.

Flashing Highly Graphitized Carbon Source. On the basis of the theoretical thermal simulations and experimental observations, we conclude that the morphology of the final product, namely the existence of tFG and wrinkled graphene, is conditional on the initial morphology of the unflashed material. Specifically, the presence of large amounts of amorphous carbon without the distinct overarching morphology is essential for the formation of tFG, owing to the high mobility of atoms. At the same time, centroid particles display low mobility of atoms and lead to the formation of the wrinkled graphene, largely maintaining its concentric shell morphology. To test this hypothesis, FG batches were generated from two carbon sources with varying amounts of amorphous carbon: (1) raw CB, and (2) previously flashed wrinkled graphene. The method by which the wrinkled graphene was treated is summarized in Figure S8a. Specifically, a batch of FG was generated by flashing for 200 ms at 120 V. The FG was then passed through a sieve with a mesh size of 150 μm. This separated the small wrinkled graphene particles from the large crystals of tFG. Figure S8b shows FG generated from flashing (left) raw CB and (right) wrinkled graphene starting materials. Notably, the FG from raw CB, which contains a much higher percentage of amorphous carbon, has more large gray crystals of tFG. The FG from the wrinkled graphene carbon does not form large area tFG crystals upon reflashing. This is further supported by the representative Raman spectra of the reflashed wrinkled graphene. It is characterized by a 2D/G ratio of slighter greater than 1.0 and characteristics similar to the wrinkled graphene starting material. Therefore, it is probable that mobile amorphous carbon is vital to form planarized tFG, and the percentage of tFG sheets formed will depend greatly on the carbon starting material.

https://dx.doi.org/10.1021/acsnano.0c05900
ACS Nano 2020, 14, 13691−13699

Effect of FJH Flash Duration. Figure S9 shows image analysis used to estimate the composition of tFG sheets and wrinkled graphene. The tFG sheets appear as gray crystals, whereas the wrinkled graphene structure appears black. Image thresholds were applied to determine the amount of gray and black material and the area of each species was used as an approximation of the composition of a batch of FG.

Figure S10 reports SEM images and representative Raman spectra for tFG sheets (gray crystals). Short pulses (10 ms) do not result in the widespread formation of tFG sheets. A percolating network of tFG is shown to form from 30−50 ms, and the Raman spectra exhibits a high 2D/G ratio indicative of tFG. Extended FJH duration (200 ms) results in the formation of a continuous layer that exhibits Raman spectra consistent with graphite. Therefore, long FJH duration gives sufficient time for AB stacking and should be avoided if the intention is to form tFG.

Figure S11 shows SEM images and Raman spectra of the wrinkled graphene morphology (black powder) from a batch of FG. The morphology does not substantially change with various FJH flash durations; however, Raman spectra reveal that the material becomes more graphitic with increasing flash duration. This is suggested by the pronounced 2D peak and the reduction of the D peak. The residual presence of the D peak is likely due to bending of the wrinkled graphene sheets.

SEM Images and Raman Spectra of tFG Sheets. Figure S12 shows SEM images of tFG sheets. This material is characterized by a faceted surface and a visible layered structure.

Figure S13 reports SEM images and Raman spectral mapping of tFG. Turbostratic crystals have pits that may indicate that the carbon source for crystallization originated from the bed of carbon particles on top of which that material crystallizes (Figure S13a). Smooth stacks of turbostratic material have high 2D/G ratio in the Raman map (Figure S13b). 2D/G ratios as high as 15.3 were observed, which is among one the largest values recorded in the literature.[1]

Some regions of tFG exhibited a morphology that was readily exfoliating as shown in Figure S14a. These regions have a representative 2D/G ratio of ∼1.3, with regions having as high a ratio as 4.69. The small D-peak suggests that this material is high-quality graphene that was readily exfoliating and only loosely bound.

Some regions from a batch of FG formed densely packed graphite polyhedral crystals (GPCs). Figure S15 shows that the GPCs form faceted rods. The Raman spectra typically displayed a 2D/G ratio of ∼1.0. Figure S16 shows more images of various GPC morphologies ranging from cones to high aspect-ratio rods. The GPC content is estimated by SEM imaging to be ∼1 wt % of the total batch of FG.

Raman Spectra of Specific Regions. To collect Raman spectra of specific morphologies, Si chips were patterned with alignment markers. This enabled single particles of FG to be found in a Raman microscope. Figure S17 shows SEM images and the corresponding Raman spectra. This confirms that the crystal shown in the SEM image is composed of tFG sheets with high 2D/G ratio (∼8). Figure S18 reports an optical image, SEM image, and Raman spectra from a particle of wrinkled graphene. This material exhibits a 2D/G ratio of ∼1 with a sizable D peak.

Mechanism of Formation. Figure S19a reports the typical power dissipation vs time curve for a batch of FG which was flashed for 200 ms. A spike in power dissipation occurs after ∼15 ms. The morphology of FG produced at various flash durations was observed and compared to this power dissipation plot in Figure 5a to to propose a mechanism for FG formation. Figure S19b shows the typical morphology after a 10 ms flash. This material does not experience the peak power dissipation and therefore does not achieve the maximum temperature (∼3000 K).[1] Raman spectra reveal incomplete graphitization of the starting material. At the peak power dissipation (∼15 ms), we propose that the junction between neighboring carbon particles rapidly heats because of the high interfacial resistance. This, then, causes the interfacial carbon to sublime, increasing the total resistance of the carbon particles, and reducing current and power dissipation at longer flash durations. Once carbon begins to sublime, the evidence suggests that faceted crystals of tFG form by 30 ms (Figure S19c) and these crystals nucleate to a percolating layer of tFG sheets by 50 ms (Figure S19d). Flashing the material for 200 ms (Figure S19e) results in the formation of a continuous graphitic film, for which Raman spectra reveals that AB-stacking occurs, an indication that the material is no longer turbostratic. Previous work has shown that sublimed carbon will form turbostratic particles similar to those seen in Figure S19c.[19] Additionally, the point of peak power dissipation must be achieved in order to find the gray crystals of tFG sheets in the batch of FG. This suggests that it is critical to drive carbon sublimation in order for the tFG sheets to form.

Exfoliated tFG Sheets. Crystals of tFG were placed on a gold substrate and subjected to shear force. This resulted in the widespread exfoliation of the material as shown in the SEM images in Figure S20. Figure S21 shows a region on a tFG crystal that was exposed to shear force. The material is readily exfoliated and wrinkles. The weak adhesion can be attributed to the turbostratic nature of the material. Figure S22 shows tFG and wrinkled graphene that was exfoliated on a Si surface. Figure S23 reports SEM images and an AFM scan taken from the same region. The thickness of the tFG is less than the surface roughness of the Au substrate and suggests monolayer or few-layer exfoliation. Raman spectra of the exfoliated tFG (Figure S24) shows a 2D/G ratio indicative of high-quality graphene and the presence of a TS1 and TS2 peak suggests that it is multilayer and turbostratic. The tFG can also be dispersed into a solvent such as oleum for exfoliation. Drop cast sheets of tFG can be seen in Figure S25.

ASSOCIATED CONTENT

Supporting Information

This is available online via the Internet at . The Supporting Information is available free of charge at https://pubs.acs.org/doi/10.1021/acsnano.0c05900.

Schematic of the FJH setup, TEM and SEM images, Raman spectra, digital images, and illustrations from atomistic simulations (PDF)

AUTHOR INFORMATION

Corresponding Authors

Boris I. Yakobson − *Department of Chemistry, Department of Materials Science and NanoEngineering, and Smalley-Curl Institute and the NanoCarbon Center, Rice University, Houston, Texas 77005, United States*; Email: biy@rice.edu

James M. Tour − *Department of Chemistry, Department of Materials Science and NanoEngineering, Smalley-Curl Institute and the NanoCarbon Center, and Department of Computer Science, Rice University, Houston, Texas 77005, United States*; orcid.org/0000-0002-8479-9328; Email: tour@rice.edu

Authors

Michael G. Stanford − *Department of Chemistry, Rice University, Houston, Texas 77005, United States*; orcid.org/0000-0001-9663-1138

Ksenia V. Bets − *Department of Materials Science and NanoEngineering, Rice University, Houston, Texas 77005, United States*; orcid.org/0000-0003-1070-3992

Duy X. Luong − *Department of Chemistry, Rice University, Houston, Texas 77005, United States*

Paul A. Advincula − *Department of Chemistry, Rice University, Houston, Texas 77005, United States*

Weiyin Chen − *Department of Chemistry, Rice University, Houston, Texas 77005, United States*

John Tianci Li − *Department of Chemistry, Rice University, Houston, Texas 77005, United States*; orcid.org/0000-0002-7218-8298

https://dx.doi.org/10.1021/acsnano.0c05900
ACS Nano 2020, 14, 13691−13699

Zhe Wang − *Department of Chemistry, Rice University, Houston, Texas 77005, United States*
Emily A. McHugh − *Department of Chemistry, Rice University, Houston, Texas 77005, United States*
Wala A. Algozeeb − *Department of Chemistry, Rice University, Houston, Texas 77005, United States*

Complete contact information is available at: https://pubs.acs.org/10.1021/acsnano.0c05900

Notes

The authors declare the following competing financial interest(s): Universal Matter, Inc., has licensed from Rice University the FJH approach to graphene. J.M.T. is a stockholder in Universal Matter but is not an employee, officer, or director. Potential conflicts of interest are mitigated through regular disclosures to and compliance with the Office of Sponsored Programs and Research Compliance at the University.

ACKNOWLEDGMENTS

We thank Vladimir Mancevski of Universal Matter, Ltd., for help with data compilation. The Air Force Office of Scientific Research (FA9550-19-1-0296) and the DOE-NETL (DE-FE0031794) funded this work. K.V.B. and B.I.Y. thank the National Science Foundation (CBET-1605848) and the Air Force Office of Scientific Research (FA9550-17-1-0262) for support.

REFERENCES

(1) Geim, A. K.; Novoselov, K. S. The Rise of Graphene. *Nat. Mater.* **2007**, *6*, 183−191.
(2) Li, X.; Cai, W.; An, J.; Kim, S.; Nah, J.; Yang, D.; Piner, R.; Velamakanni, A.; Jung, I.; Tutuc, E.; Banerjee, S. K.; Colombo, L.; Ruoff, R. S. Large-Area Synthesis of High-Quality and Uniform Graphene Films on Copper Foils. *Science* **2009**, *324*, 1312−1314.
(3) Bolotin, K.I.; Sikes, K.J.; Jiang, Z.; Klima, M.; Fudenberg, G.; Hone, J.; Kim, P.; Stormer, H.L. Ultrahigh Electron Mobility in Suspended Graphene. *Solid State Commun.* **2008**, *146*, 351−355.
(4) Balandin, A. A. Thermal Properties of Graphene and Nanostructured Carbon Materials. *Nat. Mater.* **2011**, *10*, 569−581.
(5) Papageorgiou, D. G.; Kinloch, I. A.; Young, R. J. Mechanical Properties of Graphene and Graphene-Based Nanocomposites. *Prog. Mater. Sci.* **2017**, *90*, 75−127.
(6) Marcano, D. C.; Kosynkin, D. V.; Berlin, J. M.; Sinitskii, A.; Sun, Z.; Slesarev, A.; Alemany, L. B.; Lu, W.; Tour, J. M. Improved Synthesis of Graphene Oxide. *ACS Nano* **2010**, *4*, 4806−4814.
(7) Li, X.; Magnuson, C. W.; Venugopal, A.; Tromp, R. M.; Hannon, J. B.; Vogel, E. M.; Colombo, L.; Ruoff, R. S. Large-Area Graphene Single Crystals Grown by Low-Pressure Chemical Vapor Deposition of Methane on Copper. *J. Am. Chem. Soc.* **2011**, *133*, 2816−2819.
(8) Subrahmanyam, K. S.; Panchakarla, L. S.; Govindaraj, A.; Rao, C. N. R. Simple Method of Preparing Graphene Flakes by an Arc-Discharge Method. *J. Phys. Chem. C* **2009**, *113*, 4257−4259.
(9) Gao, X.; Xu, C.; Yin, H.; Wang, X.; Song, Q.; Chen, P. Preparation of Graphene by Electrical Explosion of Graphite Sticks. *Nanoscale* **2017**, *9*, 10639−10646.
(10) Luong, D. X.; Bets, K. V.; Algozeeb, W. A.; Stanford, M. G.; Kittrell, C.; Chen, W.; Salvatierra, R. V.; Ren, M.; McHugh, E. A.; Advincula, P. A.; Wang, Z.; Bhatt, M.; Guo, H.; Mancevski, V.; Shahsavari, R.; Yakobson, B. I.; Tour, J. M. Gram-Scale Bottom-Up Flash Graphene Synthesis. *Nature* **2020**, *577*, 647−651.
(11) Harris, P. J. F.; Tsang, S. C. High-Resolution Electron Microscopy Studies of Non-Graphitizing Carbons. *Philos. Mag. A* **1997**, *76*, 667−677.
(12) Harris, P. J. F. New Perspectives on the Structure of Graphitic Carbons. *Crit. Rev. Solid State Mater. Sci.* **2005**, *30*, 235−253.
(13) Dimiev, A. M.; Ceriotti, G.; Behabtu, N.; Zakhidov, D.; Pasquali, M.; Saito, R.; Tour, J. M. Direct Real-Time Monitoring of Stage Transitions in Graphite Intercalation Compounds. *ACS Nano* **2013**, *7*, 2773−2780.
(14) Garlow, J. A.; Barrett, L. K.; Wu, L.; Kisslinger, K.; Zhu, Y.; Pulecio, J. F. Large-Area Growth of Turbostratic Graphene on Ni(111) *via* Physical Vapor Deposition. *Sci. Rep.* **2016**, *6*, 19804.
(15) Fujimoto, H. Theoretical X-Ray Scattering Intensity of Carbons with Turbostratic Stacking and AB Stacking Structures. *Carbon* **2003**, *41*, 1585−1592.
(16) Li, Z. Q.; Lu, C. J.; Xia, Z. P.; Zhou, Y.; Luo, Z. X-Ray Diffraction Patterns of Graphite and Turbostratic Carbon. *Carbon* **2007**, *45*, 1686−1695.
(17) Jenkins, G. M.; Kawamura, K. Structure of Glassy Carbon. *Nature* **1971**, *231*, 175−176.
(18) Harris, P. J. F. Fullerene-Related Structure of Commercial Glassy Carbons. *Philos. Mag.* **2004**, *84*, 3159−3167.
(19) Kokai, F.; Ishihara, M.; Koshio, A.; Nakayama, A.; Koga, Y. Fabrication of Some Graphitic Polyhedra and Balloon-Like Particles. *Diamond Relat. Mater.* **2007**, *16*, 1264−1268.
(20) Yao, Y.; Fu, K. K.; Zhu, S.; Dai, J.; Wang, Y.; Pastel, G.; Chen, Y.; Li, T.; Wang, C.; Hu, L.; et al. Carbon Welding by Ultrafast Joule Heating. *Nano Lett.* **2016**, *16*, 7282−7289.
(21) Saito, Y.; Yoshikawa, T.; Inagaki, M.; Tomita, M.; Hayashi, T. Growth and Structure of Graphitic Tubules and Polyhedral Particles in Arc-Discharge. *Chem. Phys. Lett.* **1993**, *204*, 277−282.
(22) Wang, B.; Wolfe, D.E.; Terrones, M.; Haque, M.A.; Ganguly, S.; Roy, A.K. Electro-Graphitization and Exfoliation of Graphene on Carbon Nanofibers. *Carbon* **2017**, *117*, 201−207.
(23) Harris, P. J. F.; Slater, T. J. A.; Haigh, S. J.; Hage, F. S.; Kepaptsoglou, D. M.; Ramasse, Q. M.; Brydson, R. Bilayer Graphene Formed by Passage of Current through Graphite: Evidence for a Three-Dimensional Structure. *Nanotechnology* **2014**, *25*, 465601.